1   **Interpreting the ^{13}C/^{12}C ratio of carbon dioxide in an urban airshed in the Yangtze**
2   **River Delta, China**

4   Jiaping Xu[1], Xuhui Lee[1,2*], Wei Xiao[1], Chang Cao[1], Shoudong Liu[1], Xuefa Wen[3], Jingzheng
5   Xu[1], Zhen Zhang[1], Jiayu Zhao[1]
6
7   [1]Yale-NUIST Center on Atmospheric Environment, Nanjing University of Information
8   Science & Technology, Nanjing, China
9
10   [2]School of Forestry and Environmental Studies, Yale University, New Haven, Connecticut,
11   USA
12
13   [3]Key Laboratory of Ecosystem Network Observation and Modeling, Institute of Geographic
14   Sciences and Natural Resources Research, Chinese Academy of Sciences, Beijing, China
15
16   * Corresponding author
17   Dr. Xuhui Lee
18   Sara Shallenberger Brown Professor
19   School of Forestry and Environmental Studies, Yale University,
20   21 Sachem Street, New Haven, Connecticut 06510, USA
21   Phone: (203)432-6271; Fax: (203)432-5023
22   E-mail: xuhui.lee@yale.edu

Abstract: Observations of atmospheric CO_2 mole fraction and the $^{13}C/^{12}C$ ratio (expressed as $\delta^{13}C$) in urban airsheds provide constraints on the roles of anthropogenic and natural sources and sinks in local and regional carbon cycles. In this study, we report observations of these quantities in Nanjing at hourly intervals from March 2013 to August 2015 using a laser-based optical instrument. Nanjing is the second largest city located in the highly industrialized Yangtze River Delta (YRD), Eastern China. The mean CO_2 mole fraction and $\delta^{13}C$ were (439.7 ± 7.5) µmol mol^{-1} and (-8.48 ± 0.56) ‰ over this observational period. The peak monthly mean $\delta^{13}C$ (-7.44 ‰, July 2013) was 0.74 ‰ higher than that observed at Mount Waliguan, a WMO baseline site on the Tibetan Plateau and upwind of the YRD region. The highly ^{13}C-enriched signal was partly attributed to the influence of cement production in the region. By applying the Miller-Tans method to nighttime and daytime observations to represent signals from the city of Nanjing and the YRD, respectively, we showed that the $^{13}C/^{12}C$ ratio of CO_2 sources in the Nanjing Municipality was (0.21 ± 0.53) ‰ lower than that in the YRD. Flux partitioning calculations revealed that natural ecosystems in the YRD were a negligibly small source of atmospheric CO_2.

Keywords: urban areas; CO_2 flux; Industrial process; Carbon isotope; In-situ observation

1 Introduction

Atmospheric CO_2 sources and sinks in urban areas consist mainly of plant uptake and release and fossil fuel combustion. These contributors have unique $^{13}C/^{12}C$ ratios. City clusters are human-dominated systems with high carbon emission intensity, contributing over 70% of the total anthropogenic CO_2 to the atmosphere (Satterthwaite 2008). Previous urban isotopic studies emphasize carbon emissions from fossil combustion (Zondervan and Meijer 1996, Pataki et al. 2003, Zimnoch et al. 2004, Affek and Eiler 2006, Newman et al. 2008). Relatively little attention is given to the $\delta^{13}C$ of carbon dioxide released by cement production, which is much higher than that of fossil fuel origin (Andres et al. 1994). Likewise, the CO_2 emitted from burning of minerals in non-energy consumption industrial processes, such as iron and steel production, has higher $\delta^{13}C$ than that of fossil fuel (Table 2, Widory 2006). In China, cement production and industrial processes contribute 13 % of the total anthropogenic CO_2 emission (Mu et al. 2013). Many of these industrial activities occur in or near urban areas. So far, little is known about their roles in the atmospheric carbon stable isotope budget.

One scientific motivation for quantifying the $\delta^{13}C$ of atmospheric CO_2 is that it provides constraints that allow partitioning of the net surface flux into component fluxes (Farquhar and Lloyd 1993, Yakir and Sternberg 2000, Pataki et al. 2003). The ^{13}C-based partitioning method has been used primarily for vegetation ecosystems, such as forests (Lloyd et al. 1996, Lloyd et al. 2001, Ometto, et al. 2006, Zobitz et al. 2008), grasses (Ometto et al. 2002, Pataki et al. 2003), and crops (Leavitt et al. 1995, Griffis et al. 2005). The approach has also been used in a limited number of urban studies (Pataki et al. 2003, Zimnoch et al. 2004, Newman et al.

2008, Jasek et al. 2014). Compared with vegetation ecosystems, urban ecosystems have more

complex CO_2 source configurations. We must consider both natural sources (plants and soils)

and anthropogenic sources (fossil combustion and non-energy industrial processes) and the

fact that the degree of mixing of urban air with the free troposphere and the air outside the

urban boundary varies diurnally and seasonally. Anthropogenic emissions are hard to quantify

because they depend on multiple factors including city size, population density, fossil mix,

and climate.

One of the first measurements of the carbon isotope ratio of CO_2 in an urban atmosphere

was made by Friedman and Irsa (1967). Since then, more experiments have been conducted

in urban environments (Ehleringer et al. 2002, Koerner and Klopatek 2002, Takahashi et al.

2002, Clark-Thorne and Yapp 2003, Lichtfouse et al. 2003, Widory and Javoy 2003, Zimnoch

et al. 2004, Bush et al. 2007, Guha and Ghosh 2010, Wang and Pataki 2012). The analytical

technique employed in these studies is mainly based on isotope-ratio mass-spectrometry

(IRMS). In recent years, the development of isotope ratio infrared spectroscopy (IRIS) and

on-line calibration technology provides a new solution for long-term in-situ observation of

the CO_2 mole fraction and $\delta^{13}C$ at high frequencies (1 Hz to 1 hour; Pataki et al. 2006, Griffis.

2013, Gorski et al. 2015). However, application of the IRIS technology in urban monitoring

is still limited in terms of cities covered and measurement duration (McManus et al. 2002,

Pataki et al. 2006, Wada et al. 2011, Moore and Jacobson (2015). Only a few published

studies have presented data that span one full annual cycle (e.g., Pang et al. 2016).

Simultaneous measurement of atmospheric CO_2 concentration and $\delta^{13}C$ is used to

determine the overall $^{13}C/^{12}C$ ratio of local surface sources δ_S. The majority of published

86   urban studies to date have deployed the Keeling plot method (Keeling 1958, Keeling 1961)

87   for the determination of δ_S. In this approach, a linear relationship is established between $\delta^{13}C$

88   and the reciprocal of the CO_2 mole fraction from the observed time series, and the intercept

89   of the linear regression is taken as the isotopic ratio of the local CO_2 emissions. The method

90   assumes that the isotopic ratio of the sources is invariant with time. It also assumes that

91   changes in the CO_2 mole fraction and in $\delta^{13}C$ are attributed only to the surface sources and

92   are unaffected by regional carbon sources (Pataki et al. 2003). However, these assumptions

93   do not strictly hold in an urban environment because the intensity of traffic emissions varies

94   strongly through the diel cycle (McDonald et al. 2014), and therefore the composition of the

95   surface source varies, and its $^{13}C/^{12}C$ ratio cannot be assumed constant. In addition, because

96   of strong atmospheric mixing in the daytime convective boundary layer, the background air

97   in the upper troposphere can be easily entrained to the surface layer, mixing the CO_2 that

98   originates from regional sources with that emitted locally in the urban airshed.

99   Miller and Tans (2003) propose that δ_S be determined as the slope of the linear

100   relationship

101        $\delta_a C_a - \delta_b C_b = \delta_S (C_a - C_b)$ (1)

102   where C_a is CO_2 mole fraction in urban air, C_b is CO_2 mole fraction at a background site, δ_a is

103   the $\delta^{13}C$ value of C_a, and δ_b is the $\delta^{13}C$ value of C_b. All the variables are time dependent.

104   Because this approach takes into account the fact the background atmosphere varies, it may

105   be more suitable than the Keeling method for inferring δ_S from the observations made in the

106   urban area with complex emission sources. The method has been applied to local and

107   regional carbon budget studies in nonurban settings (Miller et al. 2003) and in an urban

108 environment by Newman et al. (2016). Here we extend the method to continuous

109 measurements in an urban environment.

110 In this study, we report the results of long-term (30 months) continuous measurement of

111 atmospheric CO_2 mole fraction and $\delta^{13}C$ at a suburban site in Nanjing using an IRIS

112 instrument. Nanjing is the second largest city in the Yangtze River Delta (YRD), Eastern

113 China, with a built-up area of 753 km^2 and a population of 8.2 million. Geographically, the

114 YRD includes the provinces of Jiangsu, Zhejiang and Anhui and the Shanghai municipality

115 (29.04° to 33.41° N, 118.33° to 122.95° E) with a population of 190 million. The YRD is

116 influenced by subtropical moist monsoon climate. The mean annual temperature is about 15

117 ºC and the annual precipitation is between 1000 mm and 1800 mm. The vegetation types are

118 all C3 species. The YRD is the most industrialized region in China and had a higher urban

119 land fraction of 10.8 % as of 2014 than the global mean (2.4 %, Akbari et al. 2009). In 2014,

120 more than 220 large cement production factories (daily output exceeding 1000 tons) were

121 located in the YRD (China Cement, 2016), contributing about 20 % of the national cement

122 output.

123 The objectives of this study are (1) to characterize the atmospheric $\delta^{13}C$ diel, seasonal and

124 annual variations in this urban environment, in a region where such measurement is

125 nonexistent, (2) to investigate the influence of cement production on atmospheric $\delta^{13}C$, (3) to

126 evaluate the performance of the Keeling plot and the Miller-Tans methods for determining δ_S,

127 and (4) to explore the utility of the isotopic constraints for inferring the net surface flux and

128 the plant CO_2 flux in Nanjing and in the YRD.

129

2 Methods

2.1 Atmospheric observation

An IRIS analyzer (model G1101-i, Picarro Inc., Sunnyvale, CA) was used to measure

atmospheric CO_2 mole fraction and $^{13}C/^{12}C$ ratio ($\delta^{13}C$) continuously from February 2013 to

August 2015. The analyzer was housed on the 9th floor of our laboratory building on the

campus of Nanjing University of Information, Science and Technology (NUIST, 32°12' N,

118°43' E), in the northern suburb of Nanjing, at a linear distance of 20 km to the city center.

The instrument inlet was at a height of 34 m above the ground. There was no large industrial

CO_2 source in the 3 km radius except for a commuting road located about 300 m east of the

observation site. The nearest industrial complex, the Nanjing Iron & Steel Group Co. Ltd. and

the Nanjing Chemical Industry Group, was located about 5 km to the south of the site.

The measurement was made at 0.3 Hz and at an air flow rate of 30 mL min^{-1} at standard

temperature and pressure. One three-way solenoid valve was combined with two two-way

solenoid valves, so the analyzer could be switched for atmospheric sampling and for

sampling of two standard gases. Calibration was carried out every 3 h by sampling each

standard gas for 5 minutes following the procedure of Bowling et al. (2003) and Wen et al.

(2013). [To avoid transient effects, only the data collected in the last 2 minutes of the 5-min

calibration periods was used (Supplementary Figure S1).] Table 1 lists the concentrations and

their isotopic ratios of the standard gases used in this study. These gases were balanced in air,

and their concentration values bracketed the range of ambient concentration variability

(Figure 3 below). Their CO_2 mole fractions were measured with a gas analyzer (model

(model G1301, Picarro) and calibrated against three primary standards obtained from NOAA-

152 ESRL which were traceable to the WMO 2007 scale reported by the Central Calibration

153 Laboratory of the World Meteorological Organization, and their $\delta^{13}C$ values were measured

154 with a mass spectrometer (MAT-253, Finnigan) using IAEA reference materials IAEA-CO-8

155 (-5.76 ‰ VPDB) and IAEA-CO-9 (-47.32 ‰ VPDB). The mass spectrometer measurements

156 of these reference materials were (-5.81 ± 0.04) ‰ and (-46.64 ± 0.08) ‰. The ambient

157 measurement was averaged to hourly intervals. The isotopic ratio was expressed in the delta

158 notation ($\delta^{13}C$) in reference to the VPDB scale.

159 The typical 5-min measurement precision is 0.3 ‰ for $\delta^{13}C$ and 0.05 μmol mol^{-1} for

160 CO_2 mole fraction according to the instrument manufacturer. Our own Allan variance

161 analysis revealed a precision of 0.05 ‰ for $\delta^{13}C$ and 0.07 μmol mol^{-1} for CO_2 mole fraction at

162 the hourly averaging interval. These improvements were simply statistical, due to the increase

163 in the number of samples being used for averaging. The precision of the ambient

164 measurement was lower than this due to errors propagated through the calibration procedure.

165 According to a laboratory test on an analyzer of the same model and using the same

166 calibration procedure as ours, the hourly $\delta^{13}C$ precision is about 0.4 ‰ (Wen et al., 2013).

167 The calibration gases had much lower $\delta^{13}C$ than the ambient delta values. The mismatch

168 in the delta value between the calibration standard and the ambient air is common in

169 applications of the IRIS technique [$^{13}C(CH_4)$, Röckmann et al. 2016; $^{18}O(H_2O)$, Lee et al.

170 2005; $^{13}C(CO_2)$, Bowling et al. 2003]. For example, Bowling et al. (2003) used calibration

171 standards with delta values of -29.55 ‰ and -40.58 ‰ to calibrate their optical $^{13}C(CO_2)$

172 instrument. But because the system measures the concentrations of the major and the minor

173 isotopologue independently, it is not critical that the calibration standards and the

174   measurement target have matching isotope ratios, so long as the standards bracket

175   concentration variability of the target (Bowling et al. 2005). Nevertheless, the overall

176   accuracy of the measurement may be further improved by using calibration standards that

177   bracket variations in both the concentration and the delta values of ambient air samples. We

178   could not implement this improved calibration procedure because our analyzer failed at the

179   end of the experiment.

180   We did not adopt the strict filtering technique used for background sites (Thoning et al.

181   1989) because of high natural variations in urban airsheds. We removed the first 3 min of the

182   data after switching to the ambient sampling mode from the calibration mode. Additionally,

183   data were removed if the average hourly CO_2 mole fraction was lower than 390 μmol mol^{-1}

184   (or 30 μmol mol^{-1} lower than the midafternoon value in the summer; Figure 3 below) or $\delta^{13}C$

185   were out of the range between -15 ‰ and -5.5 ‰ (or about 3 standard deviations from the

186   mean); A total of 217 hourly values were removed by these outlier criteria.

187   The $\delta^{13}C$ value measured by the analyzer in high humidity conditions is biased high due

188   to spectral broadening and direct spectral interference (Rella 2011). To correct for the

189   humidity interference, we carried out two tests using a dew-point generator (model 610, LI-

190   COR, Inc., Lincoln, NE). A CO_2 standard gas (secondary standard gas, 439 μmol mol^{-1} in test

191   one and 488 μmol mol^{-1} in test two, balanced by dry air) was fed into the dew-point

192   generator. The outlet of the dew-point generator was connected with a 3-way union with one

193   end linked to the inlet of the analyzer and the other open to the room. The humidity level of

194   the air coming out of the dew point generator was regulated at eight levels in a dew-point

195   temperature range of 1 to 30 °C, giving a water vapor mole fraction ranging from 0.66 % to

196   4.26 % (0.66 to 4.26 cmol mol^{-1}). Measurement at each humidity level lasted 30 min, with the

197   first 5 min excluded from the analysis. Because the $^{13}C/^{12}C$ ratio of the standard gas was

198   constant, any observed variations were caused by the humidity artifact. We found that no

199   correction was needed for our analyzer if the water vapor mole fraction was below 2.03 %.

200   Above this humidity level, the measurement was biased high by 0.46 ‰ for every 1 cmol

201   mol^{-1} increase in the water vapor mole fraction (Figure 1). This humidity effect is not

202   negligible, but is an order of magnitude smaller than that reported by Rella (2011). The two

203   tests, taken eight months apart, yielded essentially the same result. The correction equation is

204        $\delta^{13}C = \delta^{13}C_{true}$ $C(H_2O) \leq 2.03$ %   (2a)

205        $\delta^{13}C = \delta^{13}C_{true} + 0.46$ ‰ $(C(H_2O)$ % $- 2.03$ %) $C(H_2O) > 2.03$ %   (2b)

206   where $C(H_2O)$ is water vapor mole fraction and was measured by the same isotope analyzer,

207    $\delta^{13}C$ is the measured isotope delta value (after the two-point calibration), and $\delta^{13}C_{true}$ is the

208   true isotope delta value. The ambient vapor mole fraction varied from 0.16 to 3.64 % during

209   the measurement period. About 35 % of the observations exceeded the threshold mole

210   fraction of 2.03 % and required correction. The largest hourly correction was 0.74 ‰. In the

211   following, all the data have been corrected for the humidity interference.

212

213   **2.2 The $^{13}C/^{12}C$ ratio of surface sources (δ_S)**

214   We applied the Miller-Tans method to estimate the $^{13}C/^{12}C$ ratio of the surface source (δ_S).

215   Strictly, Equation 1 does not allow a non-zero intercept. When applied to the urban airshed in

216   Los Angles, Equation 1 does not require an intercept (Newman et al. 2016). But when applied

217   to the data obtained at the monthly time scale in this study, the regression yielded a non-zero

218   intercept (Supplementary Figure S2). To determine if a shorter time scale would improve the

219   result, we applied the 5-h moving window technique described by Vardag et al. (2016) to the

220   observations made in January and July 2014. Only 4 % of the data, all obtained at nighttime,

221   satisfies their data screening criteria. The mean regression equation of this subset is y = (-

222   26.41 ±4.03) x + (428.84 ± 211.12) for January and y = (-25.64 ±6.39) x + (687.83 ± 264.67)

223   for July, where x is (C_a - C_b) and y is ($\delta_a C_a$ - $\delta_b C_b$). In these analyses, the background CO_2

224   mole fraction and the isotope ratio were those observed at Mount Waliguan (WLG, 36°17' N,

225   100°54' E, 3816 m above the mean sea level;

226   https://www.esrl.noaa.gov/gmd/dv/data/index.php) located at the northeastern edge of the

227   Tibetan Plateau (Zhou et al., 2005), the closest upwind WMO background station for

228   Nanjing. Use of other WMO baseline sites as the background gave essentially the same

229   results.

230   The selection of a background site is a critical issue when applying the Miller-Tans

231   method (Ballantyne et al., 2011 & 2010). That the Miller-Tans intercept does not go to zero

232   suggests that the baseline site WLG may not be a suitable background for this highly

233   urbanized region. We tested the Miller-Tans method with other isotope data published for

234   urban areas, and found that the intercept was nonzero for   the data obtained by Sturm et al.

235   (2006) at Bern, Switzerland (Supplementary Figure S3) and a number of other urban datasets

236   (Supplementary Table S1).

237   In the following, we used the tropospheric CO_2 mole ratio calculated by CarbonTracker

238   over the YRD region (altitude 3330 m; https://www.esrl.noaa.gov/gmd/dv/data/index.php) as

239   the background concentration (C_b). The CarbonTracker mole ratio is on average 3.5 µmol

240   mol^{-1} higher than that observed at WLG. To overcome the problem that CarbonTracker does

241   not calculate tropospheric $\delta^{13}C$, we rearranged Equation 1 to a form that allows an intercept

242   but without the need for a known background $\delta^{13}C$, as

243          $\delta_a C_a = \delta_S (C_a - C_b) + \delta_b C_b$ (3)

244   The $^{13}C/^{12}C$ ratio of the surface source was taken as the slope of the linear regression of $\delta_a C_a$

245   against $(C_a - C_b)$. A key difference between Equation 3 here and Equation 5 of Miller and Tans

246   (2003) is that the δ_S appears only in the slope parameter in Equation 3 but in both the slope

247   and the intercept parameter in Miller and Tans' Equation 5. This modified Miller-Tans

248   analysis requires knowledge of background CO_2 mole fraction but not δ_b.

249   The Miller-Tans analysis was performed over monthly intervals, using the data collected

250   in daytime hours (10:00 to 16:00 local time) to represent YRD and data collected during

251   nighttime hours (22:00-6:00 local time) to represent Nanjing. Morning and evening

252   transitional periods were omitted to avoid the confounding effects of sign change of the

253   biological CO_2 flux and sudden changes in the atmospheric stability regime.

254   We interpreted the daytime results to represent the influence of surface sources in the

255   YRD region and the nighttime results to represent the influence of surface sources in the

256   Nanjing municipality. The vigorous turbulent exchange in the daytime boundary layer

257   diminishes the role of local sources in the measured concentration and isotopic ratio. In other

258   words, the daytime measurement has a much larger source footprint than the size of the urban

259   land itself or the footprint of the nighttime measurement. In contrast, the buildup of CO_2 at

260   night is primarily the result of sources in the city (Shen et al. 2014), so we considered the δ_S

261   determined from the nighttime observations to represent the signal of the sources located in

262   the city. Admittedly, this interpretation of daytime versus nighttime source areas is a

263   simplification because the actual source area also depends on thermal stratification and

264   boundary layer wind. Nevertheless, it is supported by a trajectory analysis and by an analysis

265   of the atmospheric methane to CO_2 emissions ratio (Shen et al. 2014).

266   For the purpose of comparing with the Miller-Tans results, we also estimated the source

267    $^{13}C/^{12}C$ ratio using the Keeling mixing line method. According to Wehr and Saleska (2017),

268   for the measurement uncertainties of our instrument system, the ordinary least squares

269   procedure has much lower bias errors of parameter estimation than the geometric mean

270   regression. In the following, the results of both the Miller-Tans method and the Keeling

271   mixing line method were based on the ordinary least squares regression.

272

273   **2.3 Inventory of anthropogenic sources**

274   We calculated the anthropogenic CO_2 fluxes from energy consumption and industrial process

275   following the SCOPE 1 procedure issued by the International Council for Local

276   Environmental Initiatives (ICLEI, 2008). The procedure considers only emissions from

277   sources that lie within the geographic boundary of investigation. The energy consumption

278   source consists of direct emissions from the three main energy consumption sectors (industry,

279   transport, and household). We ignored the commerce sector here because the main energy

280   consumption in this sector in Nanjing and in the YRD was electric power generated by coal

281   and coal consumption which was already considered in SCOPE 1. The amounts of CO_2

282   emission were estimated with the IPCC methodology adopting the emission factors for each

283   fossil fuel type recommended by IPCC. The calculations were done separately for the YRD

284   region and for the Nanjing municipality. Because no statistical data were available for energy

285   consumption in the transport sector in Nanjing, the CO_2 emission from the transport sector

286   was deduced according to vehicle number, average annual driving distance and coefficients

287   of fuel economy (Bi et al. 2011). We obtained the data on energy consumption from official

288   sources (CESY 2013, CSY 2013, NSY, 2013).

289   The non-energy industrial processes included cement, raw iron, crude steel, and

290   ammonia synthesis processes. In the YRD, the data were available at monthly intervals. For

291   the city of Nanjing, only annual statistics were available.

292

293   **2.4 Partitioning the net surface flux**

294   We partitioned the surface CO_2 flux (F_S) into three component fluxes according to the

295   following mass conservation equations

296       $$F_S = F_F + F_C + F_P \tag{4}$$

297       $$\delta_S \, F_S = \delta_F \, F_F + \delta_C \, F_C + \delta_P \, F_P \tag{5}$$

298   where F_F is the flux from fossil fuel combustion and industrial emission except cement

299   production (termed "fossil plus"), F_C is the flux due to cement production, F_P is the biological

300   flux, and δ_F, δ_C, and δ_P are the $\delta^{13}C$ value of F_F, F_C and F_P, respectively. These CO_2 mass

301   fluxes are obtained by dividing the total emission by the surface area within the geographic

302   boundary of Nanjing or the YRD, having dimensions of mg $m^{-2} s^{-1}$. We separated the cement

303   source from other non-energy consumption industrial processes because its $^{13}C/^{12}C$ ratio is

304   much higher. In these equations, the monthly net surface flux (F_S) and the biological flux (F_P)

305   are unknowns to be solved for, and all other terms are either provided by the atmospheric

306 measurement or by the inventory calculation. The partitioning analysis was done for both

307 Nanjing and the YRD using the nighttime and daytime observations, respectively.

308 The value for δ_F was the weighted average of the isotope ratio of individual fuel types

309 and industrial processes (Table 2). The delta value of CO_2 from cement production is

310 provided by Anders (1994). We adopt a value of (-28.2 ‰) for δ_P for the YRD and Nanjing,

311 on account of a linear relationship between δ_P and tree age (Fessenden and Ehleringer 2002),

312 a typical tree age in this region (40 years) and a U-shaped relationship between δ_P and annual

313 precipitation (Pataki et al. 2007). Our δ_P is more negative than that reported for a boreal forest

314 (-26.2 ‰; Pataki et al. 2007) but is in closer agreement with the value reported for a Ginkgo

315 tree in Nanjing (-29.3 ‰; Sun et al. 2003). A summary of the isotopic ratios of the four

316 source categories is given in Table 3.

317 Uncertainties in the delta values of the different fuel types and industrial processes were

318 based on the data found in the references listed in Table 2. The uncertainty in δ_P was assumed

319 to be ± 1.00 ‰ (Verdag et al. 2016). The mass flux terms F_F and F_C were assumed to have a

320 10% uncertainty, which is typical of fossil fuel consumption data (Vardag et al. 2016).

321 To partition the nighttime flux for Nanjing, we assumed that the nighttime F_F was 20 %

322 of the daily value. The parameter 20 % was determined by the diel variation of the CO_2 flux

323 observed with an eddy covariance system in Nanjing (Bai 2011) and in several other cities

324 (Coutts et al. 2007, Song and Wang. 2011, Liu et al. 2012). At night, most of the factories in

325 the city were closed and the traffic flow was reduced to about 80 % of the daytime volume

326 (Yang et al. 2011).

327   The partitioning equations are explicit expressions of the mass balance principle. But

328 uncertainties in the isotope delta end members and the anthropogenic fluxes can propagate

329 through these equations, causing uncertainties in the estimation of F_S and F_P. Here we used a

330 Monte Carlo analysis to quantify the error propagation. The same analysis has been applied

331 to the partitioning of lake water budgets from isotope end members (Jasechko et al. 2014).

332 The procedure employed a Gaussian distribution for errors in the input variables and an

333 ensemble of 10,000 realizations for each month. Errors in F_S and F_P were computed as one

334 standard deviation of these realizations after excluding the top and bottom 50 extreme

335 ensemble members.

336

337 **3. Results**

338 **3.1. Temporal variations in the CO_2 mole fraction and $\delta^{13}C$**

339 The monthly CO_2 mole fraction during the summer was slightly lower than in the other

340 seasons (Figure 2). The mean mole fraction was 446.7 μmol mol^{-1} and 431.1 μmol mol^{-1} for

341 January and July, respectively, giving a seasonal amplitude of 15.6 μmol mol^{-1}. The mean

342 CO_2 mole fraction during the whole experimental period (March 2013 to August 2015) was

343 439.7 μmol mol^{-1}, which is 40.6 μmol mol^{-1} higher than the value observed at WLG for the

344 same period. In 2014, the calendar year with complete data coverage, the mean CO_2 mole

345 fraction was 441.2 μmol mol^{-1}, which is 42.5 ppm higher than the WLG value for the same

346 year.

347   The $^{13}C/^{12}C$ ratio of atmospheric CO_2 displayed a more clear seasonal cycle than the

348 mole fraction (Figure 2). The monthly mean value was (-9.07 ± 0.17) ‰ (mean ± standard

349   error) and (-7.63 ± 0.18) ‰ for January and July, respectively, with a seasonal amplitude of

350   1.44 ‰. The mean value for the whole experimental period was -8.48 ‰, which is the same

351   as the WLG value (-8.48 ‰). The summertime (June to August) $\delta^{13}C$ was 0.39 ‰ higher than

352   the WLG background value. The seasonality of the $^{13}C/^{12}C$ ratio at Nanjing was greater than

353   that at WLG.

354   The strongest diel variation in the CO_2 mole fraction was observed in the autumn season

355   (September to November) and the weakest in the winter season (December to February), with

356   a diel amplitude of 27.9 µmol mol^{-1} and 13.4 µmol mol^{-1}, respectively (Figure 3). In the

357   summer season, the peak value was observed at 07:00 and the lowest value at 19:00. In

358   contrast to the CO_2 mole fraction, $\delta^{13}C$ showed the lowest value in the early morning and the

359   highest value in the afternoon in all the four seasons. The diel amplitude was 1.36 ‰ in the

360   summer and 0.66 ‰ in the winter.

361

362   **3.2 $^{13}C/^{12}C$ ratio of the surface sources (δ_S)**

363   Figures 4 and 5 show an example of the modified Miller-Tans approach applied to the month

364   of January 2014. According to the slope parameter estimation, the $^{13}C/^{12}C$ ratio of the surface

365   sources was (-25.01 ± 0.90) ‰ (mean ± 95 % confidence limit) for the YRD (Figure 4) and (-

366   25.23 ± 0.74) ‰ for Nanjing (Figure 5).

367   Figure 6 shows the monthly isotopic ratio calculated with the Miller-Tans method for the

368   whole observation period. The reader is reminded here that the results obtained for the

369   daytime and the nighttime period represent sources in the YRD and in Nanjing, respectively.

370   During the two and a half years of observation, the monthly δ_S for the YRD was lower in the

371   winter [(-24.37 ± 0.71) ‰] and higher in the summer (-23.42 ± 1.79 ‰]. The seasonal

372   difference for Nanjing was smaller than for the YRD [(-24.87 ± 0.51) ‰ in the winter

373   (December to February) and -24.80 ± 1.79) ‰ in the summer months (June to August)]. The

374   sources in the YRD had slightly higher δ_S than those in in Nanjing. The mean δ_S value of the

375   whole observational period was (-24.37 ± 0.61) ‰ and (-24.58 ± 0.44) ‰ for the YRD and

376   Nanjing, respectively. The monthly δ_S for the YRD (Figure 6a) was highly correlated with the

377   monthly atmospheric $\delta^{13}C$ [Figure 2; $\delta_S = (2.29 \pm 0.78) \delta^{13}C + (-5.71 \pm 6.37)$, linear correlation

378   coefficient = 0.47, n = 30, p <0.01]. The correlation between the monthly δ_S for Nanjing

379   (Figure 6b) and the monthly atmospheric $\delta^{13}C$ was weak [$\delta_S = (2.39 \pm 0.92) \delta^{13}C + (-3.71 \pm$

380   8.07), linear correlation coefficient = 0.03, n = 30, p = 0.87]. These correlation patterns

381   suggest that atmospheric $\delta^{13}C$ was influenced more by surface sources at the regional scale

382   than at the local (city) scale.

383

384   **3.3 Inventory data for anthropogenic sources**

385   The emission strength of anthropogenic sources and their $^{13}C/^{12}C$ ratios were calculated with

386   the inventory method and the data found in the literature, as described in section 2.3. In the

387   YRD, coal combustion was by far the largest source of anthropogenic CO_2, contributing 70 %

388   of the overall "fossil-plus" emission (Table 2). Here the "fossil-plus" emission includes

389   contributions from all forms of fossil fuel combustion and from non-cement industrial

390   processes. The second and third largest source were ammonia synthesis and pig iron

391   manufacturing, with fractional contributions of about 9 %. The "fossil-plus" source

392 contribution to the total anthropogenic emission was 91 %, with the remaining 9 %

393 contributed by cement production (Table 2).

394 In the Nanjing municipality, the fractional contribution of coal to the "fossil-plus" total

395 was 52 %, lower than that for the YRD, and the other three major sources were ammonia

396 synthesis (16 %), pig iron (13 %), and gasoline (11 %). The fractional contribution of fuel-

397 plus sources to the total anthropogenic emission was 96.4 % and the fractional contribution of

398 cement production was 3.6 % (Table 2). The isotopic ratio of the "fossil-plus" sources was

399 0.35 ‰ lower for Nanjing than for the YRD.

400 The overall effective isotopic ratio of the anthropogenic sources weighted by the source

401 contributions was also lower for Nanjing than for the YRD (Table 3). The difference was

402 1.76 ‰ and was a result of lower fractional contributions in Nanjing of coal combustion and

403 cement production, which have relatively high ^{13}C contents, and a higher fractional

404 contribution of natural gas, which is the fuel type with the lowest ^{13}C content.

405

3.4. CO$_2$ fluxes in YRD and Nanjing

407 Figure 7 shows the biological flux F_P and surface flux F_S calculated from the mass balance,

408 and the cement flux F_C and "fossil-plus" F_F. The F_P flux obtained with the isotopic

409 partitioning method for the YRD agreed with the seasonal phenology expected for plants in

410 this region. It was near zero or slightly negative in the summer and generally positive in the

411 winter, indicating uptake and release, respectively. The annual mean daytime biological flux

412 was (0.03 ± 0.64) mg m^{-2} s^{-1} in the YRD in the calendar year 2014. The net surface flux F_S

413 was (0.17 ± 2.02) mg m^{-2} s^{-1} in 2014. The standard deviations of these estimates are quite

414   large. If the extreme standard deviations of F_p (5.16 mg m^{-2} s^{-1}) and F_S (22.00 mg m^{-2} s^{-1}) in

415   March 2014 were excluded, the mean standard deviation of F_p would decrease to 0.23 mg m^{-2}

416   s^{-1}for and that of F_S to 0.20 mg m^{-2} s^{-1}.

417   In Nanjing, the biological flux was positive throughout the year (Figure 8). This is

418   because the partitioning was done for the night hours when the natural ecosystems were a

419   source of CO_2 due to autotrophic and heterotrophic respiration. The annual mean nighttime

420   biological flux for the calendar year 2014 was (0.06 ± 0.26) mg m^{-2} s^{-1}. The nighttime surface

421   flux was (0.18 ± 0.22) mg m^{-2} s^{-1} in 2014.

422

423   **4 Discussion**

424   **4.1 CO_2 mole fraction and $\delta^{13}C$ seasonality**

425   The atmospheric CO_2 mole fraction observed in Nanjing showed very small seasonal

426   variation (summer versus winter difference of 7.9 μmol mol^{-1}, July versus January difference

427   of 15.6 μmol mol^{-1}), in comparison with the data published for other cities. For example, in

428   Salt Lake City, USA, the CO_2 mole fraction in the summer is about 31 μmol mol^{-1} lower than

429   in the winter (Pataki et al., 2003). Several factors contributed to the weak seasonality in

430   Nanjing. The climate in the YRD is relatively mild. The governmental energy policy prohibits

431   winter heating in public buildings. Most residential buildings also lack space heating in the

432   winter. This is in contrast to energy use patterns in northern cities in China and elsewhere.

433   The weak seasonality of the observed mole fraction was also related to the low vegetation

434   cover in the YRD and in Nanjing. The forest cover ratio is about 35 % in Nanjing and in the

435   YRD, and the overall vegetation cover (forest plus other vegetation types) ratio in the major

436 cities in the YRD is lower than 45 % (CESY, 2013; CSY, 2013). For comparison, the

437 vegetation cover ratio is 56 % in Salt Lake City (Pataki et al. 2009) and 44 % in Chicago

438 (Rose et al. 2003). Dense vegetation is known to deplete atmospheric CO_2 in the summer

439 season via photosynthetic uptake, amplifying the CO_2 seasonal amplitude.

440 Our $\delta^{13}C$ seasonal amplitude (January versus July difference of 1.44 ‰) was 4 times the

441 amplitude observed or estimated at WLG (Figure 2) but agreed with those reported by most

442 urban studies. For comparison, the seasonal amplitude of $\delta^{13}C_a$ in Bangalore, India, was 0.89

443 to 1.32 ‰ (Guha and Ghosh 2015). Similar amplitudes have also been reported for Chicago

444 (January versus August difference of 1.25 ‰; Moore and Jacobson, 2015) and Beijing

445 (2.13 ‰; Pang et al. 2016). In Salt Lake City, the seasonal amplitude of $\delta^{13}C$ was

446 approximately 1.6 ‰ because of much more natural gas consumption for heating in the

447 winter than in the summer (Pataki et al. 2006).

448

449 **4.2 Influences of cement production on atmospheric $\delta^{13}C$**

450 The high summer $\delta^{13}C$ was one of the most unique characteristics at our site. The daytime

451 $\delta^{13}C$ reached -6.90 ‰ in July 2013 and -7.21 ‰ in August 2014, which were 1.28 ‰ and

452 0.95 ‰ higher than the WLG values. The highest monthly mean $\delta^{13}C$ occurred in July: -

453 7.44 ‰ in July 2013, -7.99 ‰ in July 2014 and -7.46 ‰ in July 2015. These values were

454 0.74 ‰, 0.16 ‰ and 0.77 ‰ higher than the WLG value reported for the same months.

455 The high July values observed at our site cannot be fully explained by CO_2 removal by

456 plant photosynthesis. Photosynthesis and respiration are the two processes that dominate the

457 $^{13}C/^{12}C$ seasonality in plant-dominated landscapes, leading to higher $\delta^{13}C$ values in the

458   summer and lower values in the winter. For example, in Park Falls, Wisconsin, USA, a site in

459   a heavily-forested landscape, $\delta^{13}C$ was -7.75 ‰ in August 2011 and -8.77 ‰ in February

460   2012 (Moore and Jacobson, 2015). For comparison, $\delta^{13}C$ was -8.24‰ and -8.38 ‰ at the

461   Mauna Loa Observatory and -8.02 ‰ and -8.66 ‰ at WLG in these two months, respectively.

462   In other words, the photosynthetic effect raised the August $\delta^{13}C$ by 0.5 ‰ above the

463   background value, a smaller enrichment than observed at our site. Because of the low

464   vegetation fraction, the summer photosynthetic CO_2 uptake in the YRD and in Nanjing

465   should be lower than at Park Falls. According to the CarbonTracker inversion analysis (Peters

466   et al. 2007), the net ecosystem production at the grid point where Parks Fall is located is -

467   0.201 mg $m^{-2} s^{-1}$ in July, 2014 but is only -0.059 mg $m^{-2} s^{-1}$ at the grid point corresponding to

468   the YRD region. We would expect from the photosynthetic effect alone that the summertime

469   ^{13}C enrichment at our site to be smaller, not greater than that observed at Park Falls.

470   Furthermore, in a human-dominated landscape, the plant photosynthetic enhancement of

471   ^{13}C is offset by the CO_2 from fossil fuel combustion which has lower $^{13}C/^{12}C$ ratios than the

472   atmosphere. In Chicago, the monthly mean $\delta^{13}C$ peaked in August at -8.29 ‰ during the

473   calendar year 2011, which is 0.05 ‰ lower than the WLG value for the same month.

474   Similarly, in Beijing, the monthly mean $\delta^{13}C$ peaked at -9.49 ‰ in August 2014, which is

475   1.23 ‰ lower than the WLG value for the same month.

476   We suggest that cement production was the contributing factor responsible for the high

477    $\delta^{13}C$ values in the summer. The evidence supporting this interpretation is provided by data in

478   Table 3 and Figure 7. The delta value of anthropogenic CO_2 in the YRD would be (-26.36 ±

479   0.42) ‰ without cement production and increased to (-23.95 ± 0.41) ‰ after inclusion of the

480   cement source (Table 3). This value is much higher than those reported for other urban lands,

481   such as -30.7 ‰ for Los Angeles, USA (Newman et al. 2008) and about -31 ‰ for Salt Lake

482   City, USA (Bush et al. 2007). The overall surface source $^{13}C/^{12}C$ ratio derived from

483   atmospheric measurements (Figure 6; -24.37 ‰ and -24.58 ‰ for the YRD and Nanjing,

484   respectively) was also more enriched than those obtained from atmospheric measurements in

485   other cities, such as (-28.1 ± 0.8) ‰ for Chicago in August and September (Moore and

486   Jacobson, 2015), -32.4 ‰ to -27.4 ‰ for Salt Lake City in the growing season (Pataki et al.

487   2003), -27.0 ‰ for Beijing in the winter heating season (Pang et al. 2016), and -29.3 ‰ for

488   Los Angeles, USA (Newman et al. 2008).

489   The influence of cement production on atmospheric $\delta^{13}C$ has also been suggested for at

490   least two other urban sites. In Bangalore, India, $\delta^{13}C$ is 0.05 ‰ higher than that observed at

491   an island station in the Indian Ocean, and cement production in southern India is offered as a

492   reason to explain the enrichment of urban $\delta^{13}C$ (Guha and Ghosh 2015). The other urban site

493   is Beijing, China, where the $\delta^{13}C$ measurement may have been influenced by cement factories

494   outside the city (Ren et al. 2015, Pang et al. 2016).

495

496   **4.3 Net surface and biological fluxes in the YRD**

497   As a human-dominated landscape, the YRD was a net source of CO_2 on the monthly scale

498   even in the growing season (F_S, Figure 7). The seasonal trends of the net surface flux F_S and

499   the biological flux F_P were highly correlated with each other ($R^2 = 0.88$ after exclusion of

500   three extreme outliers) because the anthropogenic source strengths were almost constant. The

501   mean F_S between March 2013 and February 2015 was ($0.19 ± 1.16$) mg m^{-2} s^{-1}, which

502   consisted of (0.15 ± 0.02) mg m^{-2} s^{-1} from fossil combustion and industrial processes, $(0.02 \pm$

503    $0.002)$ mg m^{-2}s^{-1} from cement production and (0.05 ± 1.31) mg m^{-2} s^{-1} from biological

504   activities. The total anthropogenic CO_2 flux was (0.17 ± 0.02) mg m^{-2} s^{-1} in the YRD, a 70 %

505   increase from the value of 0.10 mg m^{-2} s^{-1} reported for 2009 (Shen et al. 2014). From 2009 to

506   2012, the GDP increased by 56 % according to the National Statistic Yearbook.

507   For comparison, we extracted the flux data from the CarbonTracker database for the 6

508   by 6 pixels that cover the YRD region. The results show that the mean daytime (11:00 to

509   17:00 local time) biological flux is slightly negative at -0.01 mg m^{-2} s^{-1} for 2014 (Peter et al.

510   2007). Our estimate of F_P for 2014 was (0.03 ± 0.64) mg m^{-2} s^{-1}. As pointed out earlier, the F_p

511   value for March 2014 was highly uncertain $[(0.21\pm 5.16)$ mg m^{-2} s$^{-1}]$; If we replace this value

512   by the mean value of February and April 2014, the 2014 mean F_P would be reduced to $(0.02 \pm$

513    $0.22)$ mg m^{-2} s^{-1}.

514   A source of uncertainty in our flux partitioning analysis is related to human breath (Affek

515   and Eiler 2006). Using the method of Prairie and Duarte (2007), we estimated that human

516   respiration flux was 0.006 and 0.013 mg m^{-2} s^{-1}, or 3.7 % and 11.65 % of anthropogenic

517   emission in the YRD and in Nanjing, respectively. The food diet in the region is

518   predominantly C3 grains. By including this additional source in Equations 3 and 4 and by

519   assuming that the isotopic ratio of digestion is the same as δ_P shown in Table 3, F_S and F_P

520   would increase by 0.008 and 0.001 mg m^{-2} s^{-1} in the YRD and by 0.018 mg m^{-2} s^{-1} and 0.005

521   mg m^{-2} s^{-1} in Nanjing, respectively.

522

523   **4.4 Comparison of the Miller-Tans and the Keeling methods**

524   By applying the Miller-Tans method to daytime and nighttime observations separately, we

525   obtained the effective source ratios that are consistent with the inventory analysis for the

526   YRD and for the Nanjing Municipality. The daytime measurement (Figure 6a, solid circles)

527   revealed that the $^{13}C/^{12}C$ ratio of the all sources (anthropogenic and biological) was on

528   average 0.21 ‰ higher than that obtained with the nighttime measurement (Figure 6b, solid

529   circles), although the difference is not statistically significant ($p = 0.38$). For comparison, the

530   overall δ_S of the anthropogenic sources in the YRD was also higher than that in Nanjing, the

531   difference being 2.01 ‰ (Table 3). The interpretation that the daytime observations capture

532   the influence of surface sources in the YRD region is supported by a trajectory analysis and

533   by an analysis of the atmospheric methane to CO_2 emissions ratio observed at the same site

534   (Shen et al. 2014). We note that the atmospheric measurements gave a smaller difference

535   between the YRD and Nanjing than that obtained by the inventory data, likely because of

536   different biological contributions between the two spatial scales.

537   One open question with regard to the modified Miller-Tans method is what constitutes

538   the true background air for the YRD. In this study, the background was assumed to be the

539   tropospheric air above the YRD. The background delta value (δ_b) backed out from the

540   intercepts shown in Figures 4 and 5 is -7.6 ‰, which is higher than expected, suggesting that

541   the true background concentration C_b may be higher than the tropospheric value. One

542   noteworthy feature about Equation 3 is that its slope parameter is not sensitive to C_b, but its

543   intercept parameter is. By increasing C_b by 15 $\mu mol\ mol^{-1}$, the slope of the regression in

544   Figure 5 would remain unchanged, but the δ_b backed out from the new intercept value would

545   become more reasonable (-8.23 ‰). In Newman et al. (2016), the background air was

measured at a coastal location upwind of the Los Angles airshed. It is recommended that a

similar strategy should be used in future experiments, where simultaneous measurement is

made at the coast of East China Sea and only data collected in easterly winds are selected for

the Miller-Tans analysis.

We also calculated the $^{13}C/^{12}C$ ratio of the surface sources with the Keeling plot method.

Using the daytime data, the Keeling result was lower and more variable than that inferred

from the Miller-Tans method using the daytime data (Figure 6a). The two methods differed

by an average of -1.51 ‰ (Supplementary Table S2).

In comparison, the Keeling plot method showed reasonably good performance when

applied to the nighttime observations. This is because surface inversion conditions effectively

prevented mixing of the free atmospheric air with the surface air, so that the single-source

assumption implicit in the Keeling plot method could be satisfied. When we applied Keeling

plot method at monthly intervals to the nighttime data, the resulting δ_S showed very similar

month-to-month variations with the value obtained with application of the Miller-Tans

method to the nighttime observations (Figure 6b). The two method differed by an average of

1.21 ‰ (Supplementary Table S2).

When the δ_S derived from the Keeling plot method was used for flux-partitioning, the

results were much more erratic than shown in Figures 7 and 8 (Supplementary Figures S4 and

S5). The uncertainty ranges of the monthly F_P and F_S were two to three times larger. The

biological flux F_P for the YRD was out of range for 4 months, and did not display an obvious

seasonal pattern (Supplementary Figure S4). These results support our choice of the modified

567   Miller-Tans method as the preferred approach for inferring the overall $^{13}C/^{12}C$ ratio of the

568   surface sources in this study.

569

570   **5. Conclusions**

571   We showed that the temporal changes of $\delta^{13}C$ followed the seasonal patterns of

572   anthropogenic and biologic CO_2 emissions, with lower values in the winter than in the

573   summer. An unusual feature that has not been seen in other urban environments is that the

574    $\delta^{13}C$ exceeded that of the background atmosphere in some of the summer months. The

575   highest monthly $\delta^{13}C$ was -7.44 ‰ observed in July 2013, which was 0.74 ‰ greater than the

576   WLG value for the same month. Evidence points to cement production as the key reason for

577   why the atmospheric $\delta^{13}C$ was higher than at the background site. In contrast to the isotope

578   ratio, the CO_2 mole fraction displayed very weak seasonality (July to January difference 15.6

579    $\mu mol\ mol^{-1}$).

580   We hypothesized that the Miller-Tans method applied to the daytime and nighttime

581   observations should yield the effective $^{13}C/^{12}C$ ratio of surface sources at the regional (YRD)

582   and the local (Nanjing) scale, respectively. According to the results of the modified Miller-

583   Tans method, the effective source $^{13}C/^{12}C$ ratio in the YRD was -24.37 ‰, which was 0.21 ‰

584   higher than that in the Nanjing Municipality. These results were consistent with inventory

585   estimates of anthropogenic source ratios at these two spatial scales.

586   By combining inventory data on anthropogenic carbon sources and the atmospheric

587   measurement of CO_2 mole fraction and $^{13}C/^{12}C$ ratio in an isotopic partitioning framework,

588   we inferred that natural ecosystems in the YRD were a negligibly small source of

589 atmospheric CO_2, with an average flux of (0.02 ± 0.22) mg m^{-2} s^{-1} for 2014. For comparison,

590 the CarbonTracker inverse analysis reveals a small annual mean daytime biological flux (-

591 0.01 mg m^{-2} s^{-1}) for this region for 2014.

592

Data availability:

594 The atmospheric data are available upon request, as an electronic supplement to the paper, or

595 from the Yale-NUIST Center website http://yncenter.sites.yale.edu.

596

Acknowledgments:

598 This research was supported by the National Natural Science Foundation of China (Grant

599 41475141, 41505005), the U. S. National Science Foundation (Grant 1520684), the Ministry

600 of Education of China (Grant PCSIRT), and the Priority Academic Program Development of

601 Jiangsu Higher Education Institutions (Grant PAPD). The first author also acknowledged a

602 visiting scholarship from China Scholarship Council and a Graduate Student Innovation

603 Grant from Jiangsu Provincial Government (Grant KYLX_0848). We thank the handling

604 editor Dr. Jan Kaiser and four anonymous reviewers whose constructive comments have

605 greatly improved this paper.

References

Affek, H. P., Eiler, J. M. (2006). Abundance of mass 47-CO_2 in urban air, car exhaust, and human breath. Geochimica et Cosmochimica Acta **70**(1): 1-12.

Akbari H, Menon S, Rosenfeld A. Global cooling: increasing world-wide urban albedos to offset CO_2. Climatic Change, 2009, **94**(3-4): 275-286.

An, H (2012) Ammonia synthesis: current status and future outlook (in Chinese), Coal Chemsitry of Western China, **2**: 4-13.

Andres, R. J., Marland, G., Boden, T., Bischof, S. (1994). Carbon dioxide emissions from fossil fuel consumption and cement manufacture, 1751-1991; and an estimate of their isotopic composition and latitudinal distribution, Oak Ridge National Lab., TN (United States);

Bai, Y., (2011) A Comparative Study on Turbulent Fluxes Exchange over Nanjing Urban and Suburban in Summer (in Chinese), Master's Thesis, Nanjing University of Information Science & Technology.

Ballantyne, A. P., Miller, J. B., Baker, I. T., Tans, P. P., White, J. W. C. (2011). Novel applications of carbon isotopes in atmospheric CO_2: what can atmospheric measurements teach us about processes in the biosphere? Biogeosciences, 8(10), 3093-3106.

Ballantyne, A. P., Miller, J. B., Tans, P. P. (2010). Apparent seasonal cycle in isotopic discrimination of carbon in the atmosphere and biosphere due to vapor pressure deficit. Global Biogeochemical Cycles, 24(3), 1-16.

Bowling, D. R., S P Burns, T. J. Conway, R. K. Monson, and J. W. C. White (2005) Extensive observations of CO_2 carbon isotope content in and above a high-elevation subalpine forest, Global Biogeochemical Cycles, **19**: GB3023.

Bi, J., Zhang, R., Wang, H., Liu, M.,Wu, Y. (2011). The benchmarks of carbon emissions and policy implications for China's cities: Case of Nanjing. Energy Policy **39**(9): 4785-4794.

Bowling, D. R., Sargent, S. D., Tanner, B. D., and Ehleringer, J. R. (2003). Tunable diode laser absorption spectroscopy for stable isotope studies of ecosystem–atmosphere CO_2 exchange, Agric. Forest Meteorol., **118:** 1–19.

Bush, S. E., Pataki, D.E., Ehleringer, J.R. (2007). Sources of variation in $\delta^{13}C$ of fossil fuel emissions in Salt Lake City, USA. Applied Geochemistry **22**(4): 715-723.

CESY (2013). China Energy Statistical Yearbook 2013: China Statistical Publishing House, Beijing. (in Chinese) Also available at: <http://www.stats.gov.cn/tjsj/ndsj/ 2013/indexch.htm>.

Clark-Thorne, S. T., C. J. Yapp (2003). Stable carbon isotope constraints on mixing and mass balance of CO2 in an urban atmosphere: Dallas metropolitan area, Texas, USA. Applied Geochemistry **18**(1): 75-95.

Coutts, A. M., Beringer, J., Tapper, N.J. (2007). Characteristics influencing the variability of urban CO_2 fluxes in Melbourne, Australia. Atmospheric Environment **41**(1): 51-62.

China Cement: http://hy.ccement.com/map/, last access: 6 July 2016 (in Chinese).

CSY (2013). China Statistical Yearbook. National Bureau of Statistics of China. (in Chinese) Also available at: <http://www.stats.gov.cn/tjsj/ndsj/2013/indexch.htm>

Duan Y. (1995) Study of characteristics of coal isotope conposition in China. Coal Geology & Exploration **23**(1) 29-33.

Ehleringer, J.R., Bowling, D.R., Flanagan, L.B., Fessenden, J.,Helliker, B., Martinelli, L.A., Ometto, J.P. (2002). Stable isotopes and carbon cycle processes in forests and grasslands. Plant biology **4**(2): 181-189.

Farquhar, G., J. Lloyd (1993). Carbon and oxygen isotope effects in the exchange of carbon dioxide between terrestrial plants and the atmosphere. Stable isotopes and plant carbon-water relations **40**: 47-70.

Fessenden, J. E., J. R. Ehleringer (2002). Age-related variations in $\delta^{13}C$ of ecosystem respiration across a coniferous forest chronosequence in the Pacific Northwest. Tree Physiology **22**(2-3): 159-167.

Friedman, L., A. P. Irsa (1967). Variations in isotopic composition of carbon in urban atmospheric carbon dioxide. Science **158**(3798): 263-264.

Gorski G, Strong C, Good S P, Bares, R., Ehleringer, J. R., Bowen, G. J. (2015). Vapor hydrogen and oxygen isotopes reflect water of combustion in the urban atmosphere. Proceedings of the National Academy of Sciences, **112**(11): 3247-3252.

Griffis, T. J., Lee, X., Baker, J.M., Sargent, S.D., King, J.Y. (2005). Feasibility of quantifying ecosystem–atmosphere $C^{18}O^{16}O$ exchange using laser spectroscopy and the flux-gradient method. Agricultural and Forest Meteorology, **135**(1-4): 44-60.

Griffis, T J. (2013). Tracing the flow of carbon dioxide and water vapor between the biosphere and atmosphere: A review of optical isotope techniques and their application. Agricultural and Forest Meteorology, **174**:85-109.

Guha, T., P. Ghosh (2010). Diurnal variation of atmospheric CO_2 concentration and delta C-13 in an urban atmosphere during winter-role of the nocturnal boundary layer. Journal of Atmospheric Chemistry, **65**(1): 1-12.

Guha, T. and P. Ghosh (2015). Diurnal and seasonal variation of mixing ratio and delta C-13 of air CO_2 observed at an urban station Bangalore, India. Environmental Science and Pollution Research, **22**(3): 1877-1890.

ICLEI (International Council for Local Environmental Initiatives). (2008). Local government operations protocol for the quantification and reporting of greenhouse gas emissions inventories. [Available online at http://www.arb.ca.gov/cc/protocols/localgov/archive/final lgo protocol 2008–09–25.pdf.]

Jasechko, S., Gibson, J. J., Edwards, T. W. (2014). Stable isotope mass balance of the Laurentian Great Lakes. Journal of Great Lakes Research, **40**(2), 336-346.

Jasek, A., Zimnoch, M., Gorczyca, Z., Smula, E., Rozanski, K. (2014). Seasonal variability of soil CO2 flux and its carbon isotope composition in Krakow urban area, Southern Poland. Isotopes in Environmental and Health Studies, **50**(2): 143-155.

Keeling, C. D. (1958). The concentration and isotopic abundances of atmospheric carbon dioxide in rural areas. Geochimica et Cosmochimica Acta, **13**(4): 322-334.

Keeling, C. D. (1961). The concentration and isotopic abundances of carbon dioxide in rural and marine air. Geochimica et Cosmochimica Acta, **24**(3): 277-298.

Koerner, B., J. Klopatek (2002). Anthropogenic and natural CO_2 emission sources in an arid urban environment. Environmental Pollution, **116**: S45-S51.

Leavitt, S. W., Paul, E.A., Galadima, A., Nakayama, F.S., Danzer, S.R., Johnson, H., Kimball, B.A. (1995). Carbon isotopes and carbon turnover in cotton and wheat FACE experiments. Plant and Soil **187**(2): 147-155.

Lee, X., Sargent, S., Smith, R., & Tanner, B. (2005). In situ measurement of the water vapor $^{18}O/^{16}O$ isotope ratio for atmospheric and ecological applications. Journal of Atmospheric and Oceanic Technology, **22**(5), 555-565.

Lichtfouse, E., Lichtfouse, M., Jaffrezic, A. (2003). delta C-13 values of grasses as a novel indicator of pollution by fossil-fuel-derived greenhouse gas CO_2 in urban areas. Environmental Science & Technology, **37**(1): 87-89.

733

734 Liu, H., Feng, J., Järvi, L., Vesala, T. (2012). Four-year (2006–2009) eddy covariance
735 measurements of CO_2 flux over an urban area in Beijing. Atmospheric Chemistry and
736 Physics, **12**(17): 7881-7892.

737

738 Lloyd, J., Kruijt, B., Hollinger, D.Y., Grace, J., Francey, R.J., Wong, S., Kelliher, F.M.,
739 Miranda, A.C., Farquhar, G.D., Gash, J.H.C. (1996). Vegetation effects on the isotopic
740 composition of atmospheric CO_2 at local and regional scales: theoretical aspects and a
741 comparison between rain forest in Amazonia and a boreal forest in Siberia. Functional Plant
742 Biology, **23**(3): 371-399.

743

744 Lloyd, J., Francey, R.J., Mollicone, D., Raupach, M.R, Sogachev, A., Arneth, A., Byers, J.N.,
745 Kelliher, F.M., Rebmann, C., Valentini, R. (2001). Vertical profiles, boundary layer budgets,
746 and regional flux estimates for CO_2 and its $^{13}C/^{12}C$ ratio and for water vapor above a
747 forest/bog mosaic in central Siberia. Global Biogeochemical Cycles, **15**(2): 267-284.

748

749 McDonald, B.C., McBride, Z. C., Martin, E. W., Harley, R. A. (2014). High-resolution
750 mapping of motor vehicle carbon dioxide emissions. Journal of Geophysical Research:
751 Atmospheres, **119**(9): 5283-5298.

752

753 McManus, J. B., Zahniser, M.S., Nelson, D.D., Williams, L.R., Kolb, C.E. (2002). Infrared
754 laser spectrometer with balanced absorption for measurement of isotopic ratios of carbon
755 gases. Spectrochimica Acta Part A: Molecular and Biomolecular Spectroscopy, **58**(11): 2465-
756 2479.

757

758 Miller, J. B., P. P. Tans (2003). Calculating isotopic fractionation from atmospheric
759 measurements at various scales, Tellus B, **55**(2): 207-214.

760

761 Miller, J.B., Tans, P.P., White, J.W.C., Conway, T.J., Vaughn, B.W. (2003). The atmospheric
762 signal of terrestrial carbon isotopic discrimination and its implication for partitioning carbon
763 fluxes, Tellus B, **55**(2): 197-206.

764

765 Moore J., Jacobson A.D. (2015). Seasonally varying contributions to urban CO_2 in the
766 Chicago, Illinois, USA region: Insights from a high-resolution CO_2 concentration and $d^{13}C$
767 record. Elementa: Science of the Anthropocene, **3**: 000052.

768

769 Mu, H., Li, H., Zhang, M., Li, M. (2013). Analysis of China's carbon dioxide flow for 2008.
770 Energy Policy **54**: 320-326.

771

772 Newman, S., Xu, X., Gurney, K.R., Hsu, Y.K., Li, K.F., Jiang, X., Keeling, R., Feng, S.,
773 O'Keefe, D., Patarasuk, R. and Wong, K.W. (2016). Toward consistency between trends in
774 bottom-up CO_2 emissions and top-down atmospheric measurements in the Los Angeles
775 megacity. Atmospheric Chemistry and Physics, **16**(6):3843-3863.

776

777

778 Newman, S., Xu, X., Affek, H.P., Stolper, E., Epstein, S. (2008). Changes in mixing ratio and
779 isotopic composition of CO2in urban air from the Los Angeles basin, California, between
780 1972 and 2003, Journal of Geophysical Research, **113**(D23): 1-15.

781

782 NSY (2013). Nanjing Statistical Yearbook. Nanjing Municipal Bureau Statistics. (in Chinese)
783 Also available at: < http://www.njtj.gov.cn/2004/2013/renmin/index.htm>

784

785 Ometto, J. P., Flanagan, L.B., Martinelli, L.A., Moreira, M.Z., Higuchi, N., Ehleringer, J.R.
786 (2002). Carbon isotope discrimination in forest and pasture ecosystems of the Amazon Basin,
787 Brazil, Global Biogeochemical Cycles, **16**(4):1-10.

788

789 Ometto, J.P., Ehleringer, J.R., Domingues, T.F., Berry, J.A., Ishida, F.Y., Mazzi, E., Higuchi,
790 N., Flanagan, L.B., Nardoto, G.B., Martinelli, L.A. (2006). The stable carbon and nitrogen
791 isotopic composition of vegetation in tropical forests of the Amazon Basin, Brazil,
792 Biogeochemistry, **79**(1-2): 251-274.

793

794 Pan, J. (2007) Theoretical and Process Studies of the Abatement of Fuel Gas Emissions
795 during Iron Ore Sintering (in Chinese), PhD Dissertation, Southcentral Univeristy of China.

796

797 Pang, J., Wen, X., Sun, X. (2016). Mixing ratio and carbon isotopic composition investigation
798 of atmospheric CO_2 in Beijing, China. Sci Total Environ, **539**: 322-330.

799

800 Pataki, D. E., Bowling, D.R., Ehleringer, J.R. (2003). Seasonal cycle of carbon dioxide and
801 its isotopic composition in an urban atmosphere: Anthropogenic and biogenic effects. Journal
802 of Geophysical Research-Atmospheres, **108**(D23): 1-8.

803

804 Pataki, D. E., Bowling, D.R., Ehleringer, J.R., Zobitz, J.M. (2006). High resolution
805 atmospheric monitoring of urban carbon dioxide sources. Geophysical Research Letters,
806 **33**(3): 1-5.

807

808 Pataki, D. E., Ehleringer, J.R., Flanagan, L.B., Yakir, D., Bowling, D.R., Still, C.J.,
809 Buchmann, N., Kaplan, J.O., Berry, J.A. (2003). The application and interpretation of Keeling
810 plots in terrestrial carbon cycle research. Global Biogeochemical Cycles, **17**(1): 1-14

811

812 Pataki, D. E., Lai, C., Keeling, C.D., Ehleringer, J.R. (2007). Insights from stable isotopes on
813 the role of terrestrial ecosystems in the global carbon cycle. Terrestrial Ecosystems in a
814 Changing World, Springer: 37-44.

815

816 Pataki,D.E., Emmi,P.C., Forster,C.B., Mills,J.I., Pardyjak,E.R., Peterson,T.R.,
817 Thompson,J.D., Dudley-Murphy,E., An integrated approach to improving fossil fuel
818 emissions scenarios with urban ecosystem studies. Ecological Complexity, 2009, **6**(1): 1-14.

819

Peters,W., Jacobson, A.R., Sweeney, C., Andrews, A.E., Conway, T.J., Masarie, K., Miller, J.B., Bruhwiler, L.M., Petron, G., Hirsch, A.I., Worthy, D.E., van der Werf, G.R., Randerson, J.T., Wennberg, P.O., Krol, M.C., Tans, P.P. (2007) An atmospheric perspective on North American carbon dioxide exchange: CarbonTracker, Proceedings of the National Academy of Sciences, **104**(48): 18925-18930.

Prairie, Yves T., Duarte, C. M. (2007). Direct and indirect metabolic CO_2 release by humanity. Biogeosciences, **4**(2): 215-217.

Rella, C. (2011). Accurate stable carbon isotope ratio measurements with rapidly varying carbon dioxide concentrations using the Picarro $\delta^{13}C$ G2101-i gas analyzer, Picarro White Paper. Picarro Inc.

Ren, L., Wang, W., Wang, J., Liu, R. (2015). Analysis of energy consumption and carbon emission during the urbanization of Shandong Province, China. Journal of Cleaner Production, **103**: 534-541.

Röckmann1 T, S Eyer, C. van der Veen1, ME Popa, B Tuzson, G Monteil1, S Houweling, Eliza Harris, D Brunner, H Fischer, G Zazzeri, D Lowry, EG Nisbet, WA Brand, JM Necki, L Emmenegger, and J Mohn (2016). In situ observations of the isotopic composition of methane at the Cabauw tall tower site. Atmos. Chem. Phys., **16**: 10469–10487.

Rose L S, Akbari H, Taha H. Characterizing the fabric of the urban environment: a case study of Greater Houston, Texas. Lawrence Berkeley National Laboratory, 2003.

Satterthwaite D. Cities' contribution to global warming: notes on the allocation of greenhouse gas emissions. Environment and Urbanization, 2008, **20**(2): 539–549.

Shen, S., Yang, D., Xiao, W., Liu, S., Lee, X. (2014). Constraining anthropogenic CH_4 emissions in Nanjing and the Yangtze River Delta, China, using atmospheric CO_2 and CH_4 mixing ratios, Advances in Atmospheric Sciences, **31**(6): 1343-1352.

Song, T., Wang Y. (2012). Carbon dioxide fluxes from an urban area in Beijing. Atmospheric Research, **106**: 139-149.

Sturm, P., Leuenberger, M., Valentino, F. L., Lehmann, B. and Ihly B. (2006). Measurements of CO_2, its stable isotopes, O_2/N_2, and ^{222}Rn at Bern, Switzerland. Atmos. Chem. Phys., **6**: 1991–2004.

Sun, B., Dilcher, D.L., Beerling, D.J., Zhang, C., Yan, D., Kowalski, E. (2003). Variation in Ginkgo biloba L. leaf characters across a climatic gradient in China. Proceedings of the National Academy of Sciences, **100**(12): 7141-7146.

Takahashi, H. A., Konohira, E., Hiyama, T., Minami, M., Nakamura, T., Yoshida, N. (2002). Diurnal variation of CO_2 concentration, Delta C-14 and delta C-13 in an urban forest: estimate of the anthropogenic and biogenic CO_2 contributions, Tellus B, **54**(2): 97-109.

Tans, P. (1981). $^{13}C/^{12}C$ of industrial CO^2. In SCOPE 16: Carbon Qcle Modelling (B.Bolin, ed.), John Wiley and Sons, Chichester, England, 127-129.

Thoning, K. W., Tans, P.P., Komhyr, W.D. (1989). Atmospheric carbon dioxide at Mauna Loa Observatory: 2. Analysis of the NOAA GMCC data, 1974–1985. Journal of Geophysical Research, **94**(D6): 8549-8565.

Sanam Noreen Vardag, S. N., S. Hammer, I. Levin (2016) Evaluation of 4 years of continuous $^{13}C(CO_2)$ data using a moving Keeling plot method, Biogeosciences, Biogeosciences, **13**: 4237–4251.

Wada, R., Nakayama, T., Matsumi, Y., Hiyama, T., Inoue, G., Shibata, T. (2011). Observation of carbon and oxygen isotopic compositions of CO_2 at an urban site in Nagoya using Mid-IR laser absorption spectroscopy. Atmospheric Environment, **45**(5): 1168-1174.

Wang, D. (2013) Method and Empirical Research of Urban Greenhouse Gas Measurement (in Chinese), Master's Thesis, Tianjin University.

Wang, W. , D. E. Pataki (2012). Drivers of spatial variability in urban plant and soil isotopic composition in the Los Angeles basin. Plant and Soil, **350**(1-2): 323-338.

Wen, X. F., Meng, Y., Zhang, X., Sun, X., Lee, X. (2013). Evaluating calibration strategies for isotope ratio infrared spectroscopy for atmospheric $^{13}CO_2/^{12}CO_2$ measurement. Atmospheric Measurement Techniques, **6**(1): 795-823.

Wehr, R., and S. R. Saleska (2017) The long-solved problem of the best-fit straight line: application to isotopic mixing lines, Biogeosciences, **14**: 17-29.

Widory, D. (2006). Combustibles, fuels and their combustion products: A view through carbon isotopes. Combustion Theory and Modelling, **10**(5): 831-841.

Widory, D., M. Javoy (2003). The carbon isotope composition of atmospheric CO_2 in Paris. Earth and Planetary Science Letters, **215**(1-2): 289-298.

Yakir, D., L. da SL Sternberg (2000). The use of stable isotopes to study ecosystem gas exchange. Oecologia, **123**(3): 297-311.

Yang, H.M., Wang, H.Z. , Wu, Y.B. (2011). Observation and characteristics analysis of traffic flow in Nanjing. (in Chinese), Environmental Science and Technology, **24**(2): 98-101.

907 Zimnoch, M., Florkowski, T., Necki, J. M., Neubert, R. E. (2004). Diurnal variability of $\delta^{13}C$
908 and $\delta^{18}O$ of atmospheric CO_2 in the urban atmosphere of Kraków, Poland. Isotopes in
909 Environmental and Health Studies, **40**(2), 129-143.
910
911 Zobitz, J. M., Burns, S.P., Reichstein, M., Bowling, D.R. (2008). Partitioning net ecosystem
912 carbon exchange and the carbon isotopic disequilibrium in a subalpine forest. Global Change
913 Biology, **14**(8): 1785-1800.
914
915 Zondervan, A., H. A. Meijer (1996). Isotopic characterisation of CO_2 sources during regional
916 pollution events using isotopic and radiocarbon analysis. Tellus B, **48**(4): 601-612.
917
918 Zhou, L., Conway, T.J., White, J.W., Mukai, H., Zhang, X., Wen, Y., Li, J. and MacClune, K.,
919 (2005). Long-term record of atmospheric CO_2 and stable isotopic ratios at Waliguan
920 Observatory: Background features and possible drivers, 1991–2002. Global Biogeochemical
921 Cycles, **19**(3): GB3021.
922

923 **Figure 1**. Dependence of the observed $\delta^{13}C$ on the H_2O mole fraction. The lines represent
924 Equation 2. Error bars are ± one standard deviation of 1-min averages. The data in the left
925 panel was obtained on October 1, 2014 using a 439 μmol mol^{-1} standard gas and the true $\delta^{13}C$
926 value of -32.8 ‰, and that in the right panel on June 10, 2015 using a 488 μmol mol^{-1}
927 standard gas and the true $\delta^{13}C$ value of -34.1 ‰.

928
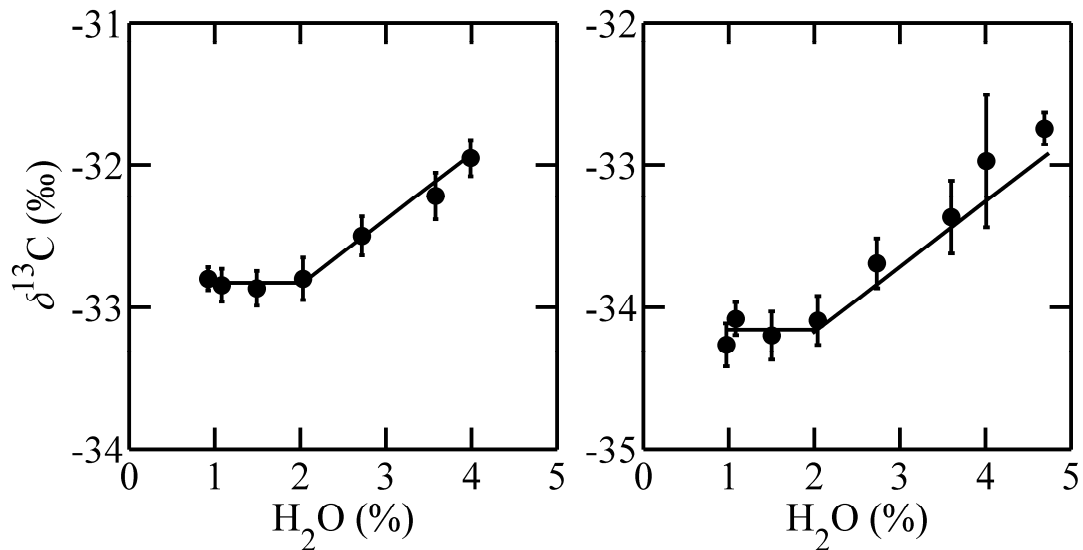
929

930   **Figure 2.** Monthly total CO_2 mole fraction (upper panel) and $\delta^{13}C$ (lower panel): Solid lines

931   with circles: whole-day means; dashed lines with up triangles: daytime (10:00-16:00) means;

932   dashed line with down triangles: nighttime (22:00-6:00) means; smooth solid lines, monthly

933   means observed at WLG.
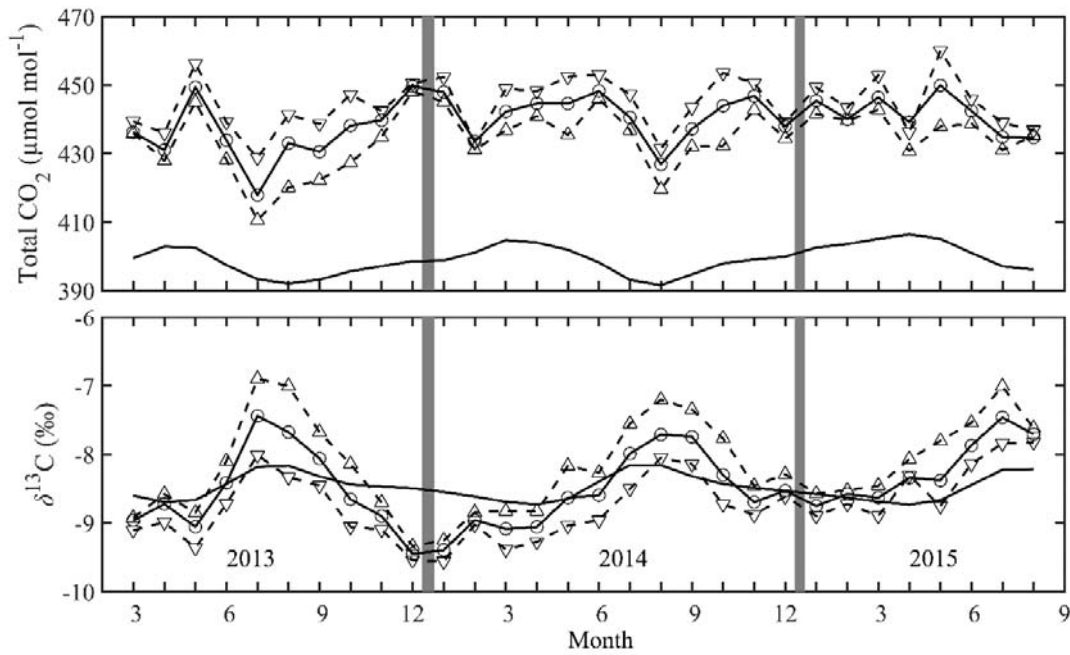
934

935

936

937   **Figure 3**. Mean diel variation of the CO_2 mole fraction (upper panels) and the $\delta^{13}C$ value

938   (bottom panels) between March, 2013 and August, 2015.
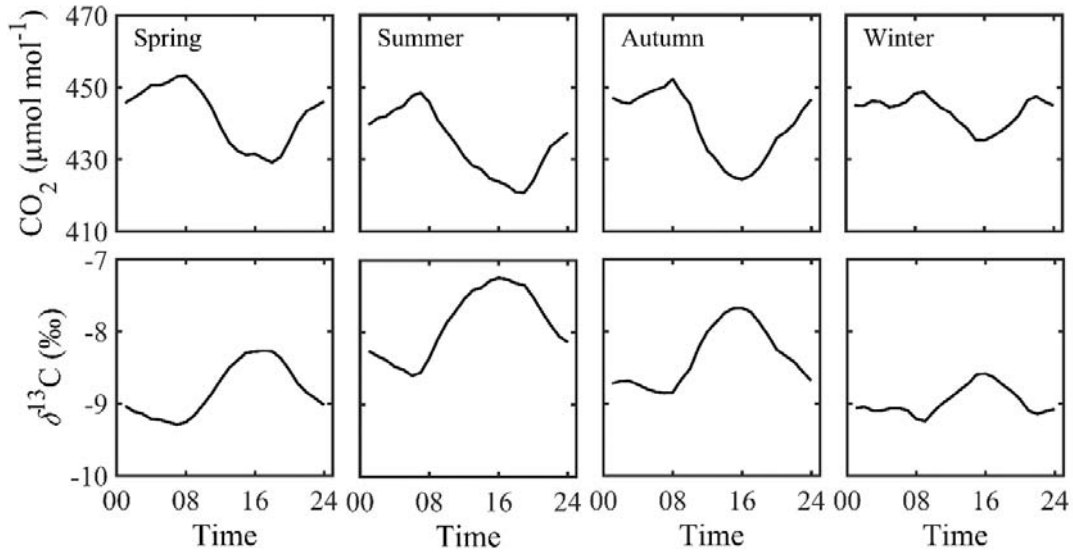
939
940

941   **Figure 4**. Application of the Miller-Tans method to the daytime (10:00-16:00) data obtained

942   in January 2014. Each data point is one hourly mean. The solid line is the least squares

943   regression according to Equation 3. Errors bounds on the regression coefficients are 95 %

944   confidence intervals.
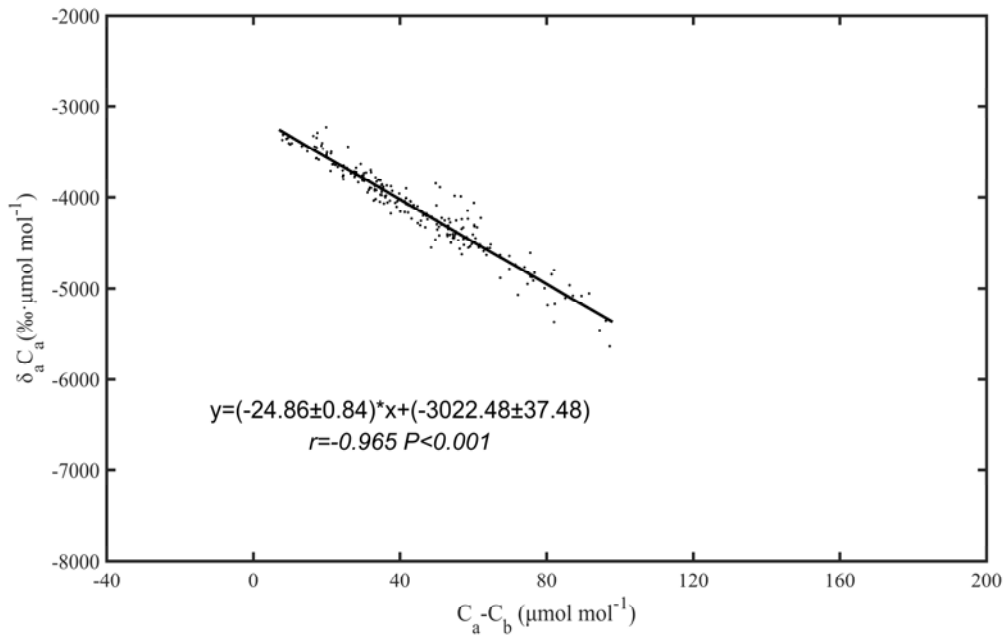
945

946 **Figure 5**. Same as Figure 4 but for nighttime (22:00-6:00) data obtained in January 2014.
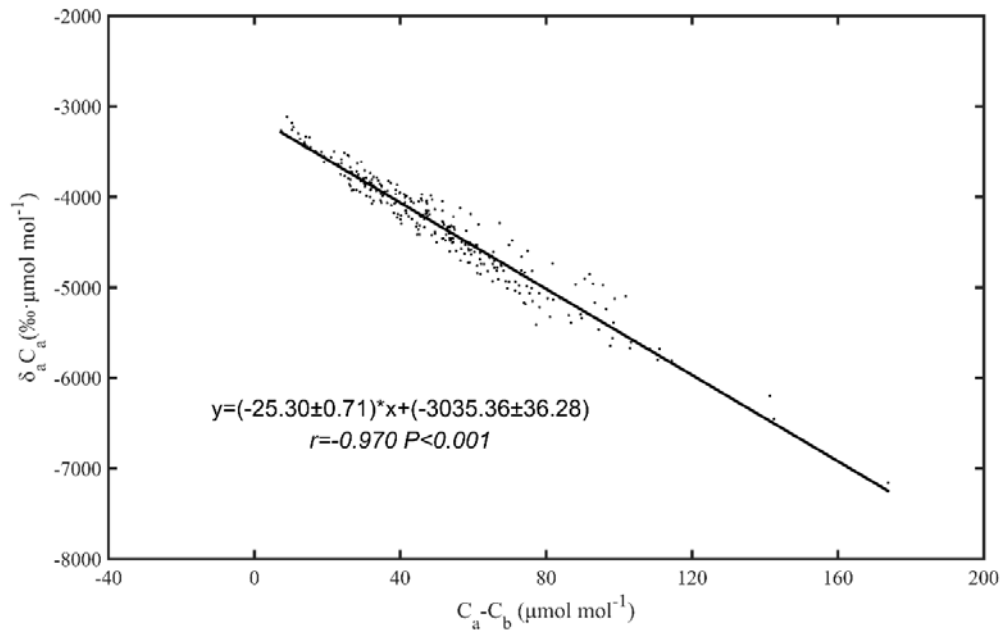
947

948   **Figure 6**. Time series of monthly $^{13}C/^{12}C$ ratio of surface sources in the YRD (a) and in

949   Nanjing (b), obtained from daytime and nighttime measurement, respectively. The error bars

950   are ± one standard deviation of the regression coefficient.
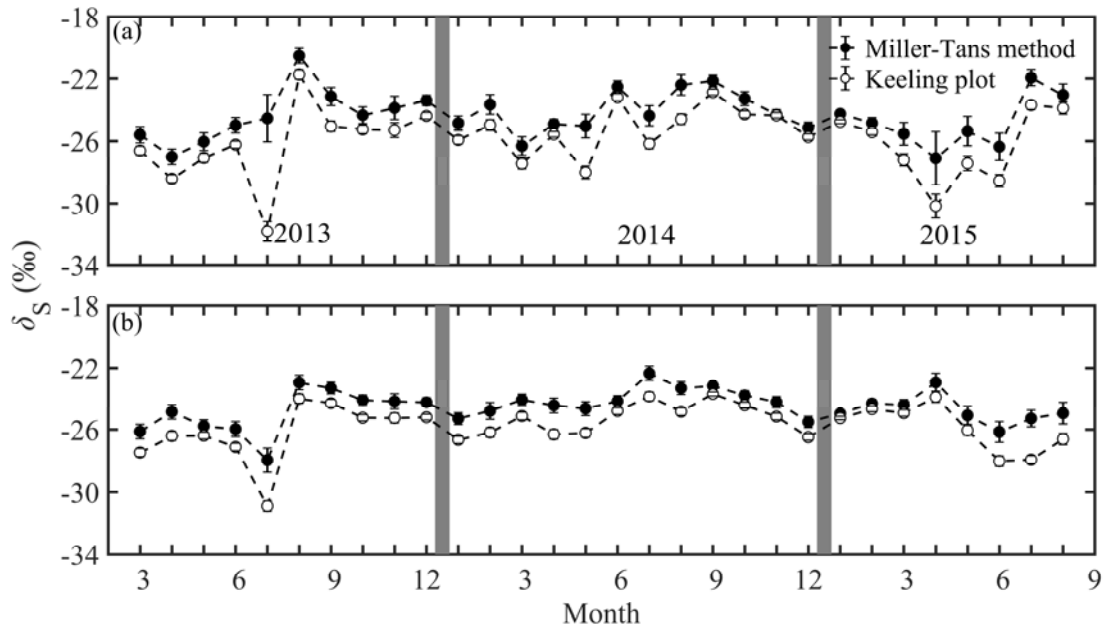
951

952

953

954

955   **Figure 7**. Time series of monthly net surface CO_2 flux (F_S), biological CO_2 flux (F_P),

956   anthropogenic CO_2 flux excluding cement emission (F_F) and cement CO_2 flux (F_c) in the

957   YRD. All the CO_2 mass fluxes are in mg m^{-2} s^{-1}. The flux terms F_F and F_c are assumed to have

958   a 10 % uncertainty typical of fossil fuel consumption data. The partitioning results (F_P and

959   F_S) are based on the source $^{13}C/^{12}C$ ratio derived from daytime atmospheric measurements.
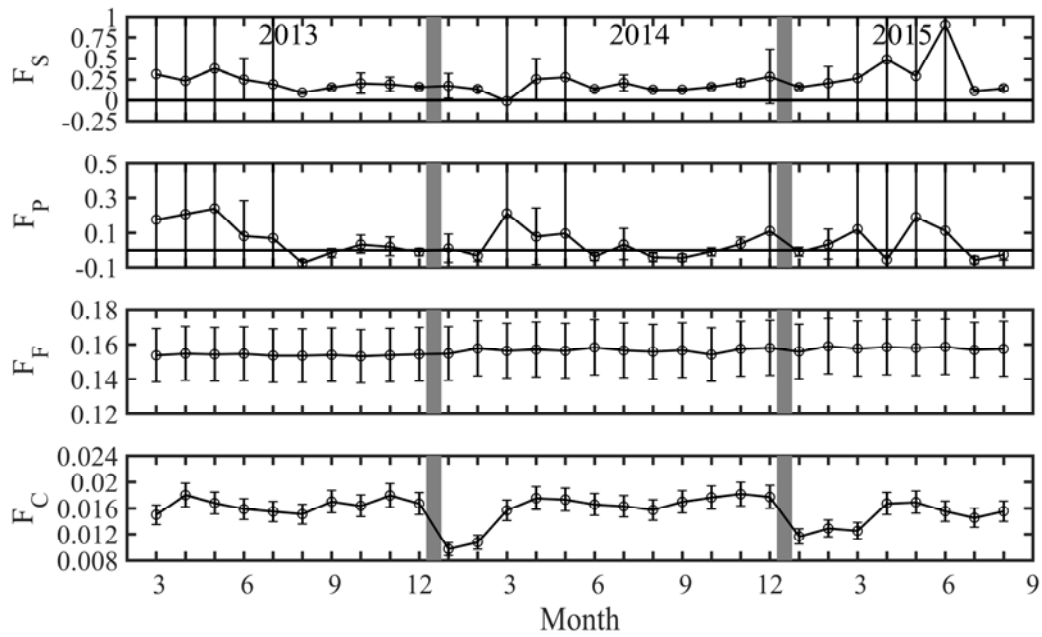
960
961

962   **Figure 8**. Time series of monthly net surface CO_2 flux (F_S), biological CO_2 flux (F_P),

963   anthropogenic CO_2 flux excluding cement emission (F_F) and cement CO_2 flux (F_c) in

964   Nanjing. All the CO_2 mass fluxes are in mg m^{-2} s^{-1}. The flux terms F_F and F_c are assumed to

965   have a 10 % uncertainty typical of fossil fuel consumption data. The partitioning results (F_P

966   and F_S) are based on the source $^{13}C/^{12}C$ ratio derived from nighttime atmospheric

967   measurements.

968
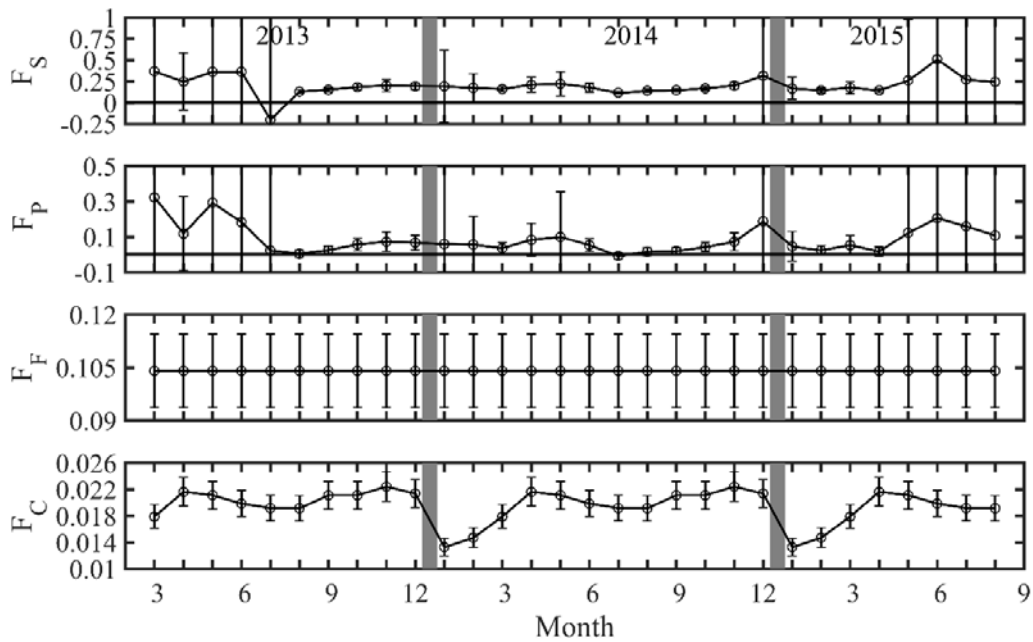
969

970 **Table 1** Standard gases used for instrument calibration. The mean and standard deviation of

971 the CO_2 mole fraction and $\delta^{13}C$ were based on 6 and 5 repeated measurements, respectively.

ID	CO_2 (μmol mol^{-1})	$\delta^{13}C$ (‰)	Period
1 Low	381.89 ± 0.99	-29.75 ± 0.27	Mar, 2013 - Aug, 2014
1 High	502.35 ± 0.28	-30.01 ± 0.18	Mar, 2013 - Aug, 2014
2 Low	380.92 ± 0.95	-29.75 ± 0.27	Sep, 2014 - Aug, 2015
2 High	501.05 ± 0.33	-30.01 ± 0.18	Sep, 2014 - Aug, 2015

972

973   **Table 2** Percentage of "fossil-plus" sources and their δ^{13}C values for the YRD and Nanjing.

974   The uncertainty in the total "fossil-plus" source is a weighted mean of the individual

975   uncertainties.

Sources	Percentage (%)		δ^{13}C (‰)		References
	YRD	Nanjing	YRD	Nanjing	
Coal	70.0	52.3	-25.46 ± 0.39	-25.46 ± 0.39	Duan, 1995, Widory 2003
Gasoline	2.1	11.4	-28.69 ± 0.50	-28.69 ± 0.50	Widory and Javoy 2003
Diesel	3.2	1.6	-28.93 ± 0.26	-28.93 ± 0.26	Widory 2006
Fuel oil	2.1	0.3	-29.32 ± 0.15	-29.32 ± 0.15	Widory and Javoy 2003
Natural gas	2.7	5.0	-39.06 ± 1.07	-39.06 ± 1.07	Widory 2003
LPG	0.7	0.2	-31.70 ± 0.40	-31.70 ± 0.40	Widory 2006
Pig iron	8.7	12.7	-24.90 ± 0.40	-24.90 ± 0.40	Pan 2007
Crude steel	1.5	0.7	-25.28 ± 0.40	-25.28 ± 0.40	Wang 2013
Ammonia synthesis	9.0	15.9	-28.18 ± 0.55	-28.18 ± 0.55	An 2012
Total	100	100	-26.36 ± 0.42	-26.97 ± 0.46	

976

977 **Table 3**. Inventory data for the isotopic composition of surface CO_2 sources and their

978 percentage of contribution in the YRD and in Nanjing. Here the "fossil-plus" category

979 includes all non-cement anthropogenic emissions listed in Table 2. The cement isotopic ratio

980 is based on Andres et al. (1994). The uncertain range in the biological isotope ratio is based

981 on Vardag et al. (2016).

Sources	YRD		Nanjing	
	$\delta^{13}C$ (‰)	Percentage (%)	$\delta^{13}C$ (‰)	Percentage (%)
"Fossil-plus"	-26.36 ± 0.42	91.0	-26.97 ± 0.46	96.4
Cement	0 ± 0.30	9.0	0 ± 0.30	3.6
Anthropogenic	-23.99 ± 0.41	100	-26.00 ± 0.45	100
Biological	-28.20 ± 1.00	——	-28.20 ± 1.00	——

982